Joint RIS Assignment and Entanglement Distribution With Purification in FSO-Based Quantum Networks

Chun-An Yang[§‖], Yung-Hsiang Chang[†‖], Jing-Jhih Du[†], Juliette Chou Le Touze[†],
Jian-Jhih Kuo[†*], Chih-Yu Wang[‡], and Ming-Jer Tsai[§]
[§]Dept. of Computer Science, National Tsing Hua University, Hsinchu, Taiwan
[†]Dept. of Computer Science and Information Engineering, National Chung Cheng University, Chiayi, Taiwan
[‡]Research Center for Information Technology Innovation, Academia Sinica, Taipei City, Taiwan

***Abstract*—Terrestrial free-space optical (FSO)-based quantum networks (QNs) have been regarded as a viable alternative to overcome the scalability and service availability limitations of fiber- or satellite-based QNs. However, FSO channels require line-of-sight connections between quantum base stations (QBSs) and user equipments (UEs), making them highly susceptible to blockage by obstacles. Reconfigurable intelligent surfaces (RISs) have emerged as a promising solution by dynamically redirecting optical links to maintain connectivity. Despite their potential, RIS-assisted quantum transmissions pose challenges, including limited QBS capacity, fidelity degradation, UE demand requirements, and RIS assignments. To address these challenges, we formulate an optimization problem and propose a 2-approximation algorithm that jointly determines UE-RIS assignment and entanglement distribution while incorporating entanglement purification. Finally, simulation results demonstrate that our proposed algorithm outperforms existing baselines by up to 67%.**

I. Introduction

Quantum networks (QNs) have been validated to facilitate secure data transmission and quantum information processing [1], [2]. Most existing research on QNs has focused on fiber- or satellite-based architectures [3]–[5]. However, the former suffers from high deployment costs [6], and the latter faces challenges such as limited availability under adverse weather conditions and limited flexibility in dense urban environments [6]. These limitations motivate the exploration of *terrestrial free-space optical (FSO)-based QNs* [7], [8], where quantum base stations (QBSs) on the ground generate entanglement and wirelessly transmit quantum optical signals to user equipments (UEs), providing more reliable and adaptable entanglement distribution over moderate distances. Compared to wireline connections, ground-based FSO channels offer lower signal loss over similar distances and avoid the need for costly physical infrastructure [6]. Nevertheless, establishing FSO channels between the QBS and UEs remains difficult, as line-of-sight (LoS) paths can be blocked by obstacles. In addition, atmospheric turbulence can cause beam deflection, reducing the probability of successful entanglement distribution [6].

To address the LoS limitations in FSO-based QNs, recent studies have begun exploring the use of *reconfigurable intelligent surface (RIS)* into FSO-based QNs [9], [10], which have

‖: equal contributions; *: corresponding author (lajacky@cs.ccu.edu.tw)
This work was supported in part by the National Science and Technology Council, Taiwan, under Grants 111-2221-E-007-044-MY3, 111-2628-E-194-001-MY3, 113-2221-E-194-040-MY3, 114-2628-E-194-002-MY3, and 114-2221-E-007-079-, and the Academia Sinica under Thematic Research Grant AS-TP-110-M07-3 in Taiwan.

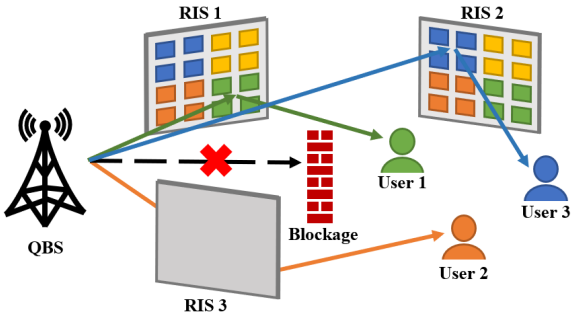

Fig. 1. Quantum network with RIS-assisted scheme.

been shown to enhance spectral efficiency and link reliability in classical wireless communications by dynamically adjusting phase shifts of incoming optical waves at low energy cost [11]. Unlike active relays, RISs deployed in FSO-based QNs forward entangled pairs without requiring quantum memory, enabling cost-effective and low-latency entanglement distribution [10]. Moreover, a RIS can be partitioned into multiple sub-surfaces [12], each of which independently reflects signals toward different UEs to further improve entanglement distribution efficiency. Fig. 1 illustrates a novel RIS-assisted FSO-based QN, where a QBS distributes entangled pairs to UEs. When direct LoS paths are blocked by obstacles, intermediate RISs redirect optical signals toward the UEs, creating virtual LoS paths on demand and significantly increases service availability.

While RISs can establish virtual LoS paths for distributing entangled pairs, they inevitably increase the overall transmission distances. Longer distances exacerbate decoherence effects and reduce the fidelity of entangled pairs. As the reduced fidelity falls below the UEs' required fidelity threshold, *entanglement purification* [13] can be employed, which consumes additional sacrificial entangled pairs to enhance the fidelity of target pairs. Fig. 2 illustrates the entanglement purification process, where the initial fidelity of an entangled pair $(\overline{v_1 v_2})$ is 0.76, below the required fidelity threshold of 0.8. A purification round is performed by consuming an additional sacrificial entangled pair (indicated by the dotted red line), improving the fidelity of $(\overline{v_1 v_2})$ to 0.91 and meeting the fidelity threshold. The purification can be applied repeatedly on the same target pair by progressively sacrificing more entangled pairs (i.e., resources) in each round until the fidelity threshold is satisfied.

The system aims to maximize the total weighted demand size by distributing entangled pairs to UEs with strict fidelity thresholds and hard demand constraints—the fidelity and rate

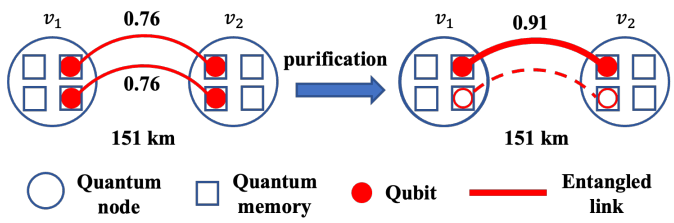

Fig. 2. Purification process.

of entanglement pairs received by each UE must fully satisfy its requirement, or such a requirement is considered unmet—where each UE has a weight reflecting its priority. These factors lead to a non-trivial optimization problem, characterized by several fundamental challenges: 1) *Distance-fidelity trade-off under probabilistic success*. To meet the required fidelity thresholds, UEs with longer paths may require more entanglement purification rounds, consuming more entangled pairs. As a result, the system must carefully balance the trade-off between allocating resources to UEs suffering from reduced fidelity and preserving capacity to serve more UEs. 2) *Limited capacity versus hard user demands*. Each UE specifies a hard demand for the expected number of successfully established entangled links, which must be fully satisfied. However, the QBS has a limited entanglement generation rate. Therefore, the allocation must balance resource consumption carefully to maximize the total demand size of satisfied UEs. 3) *Value-weighted resource allocation across multi-path options*. Each weighted UE has one or more paths from the QBS, each with a different cost and success probability. The system must jointly assign RISs and allocate resources under various trade-offs.

In the literature, the RIS assignment, entanglement distribution, and entanglement purification in QNs were solved separately [10], leading to suboptimal solutions.[1] To address these challenges, we formulate a novel optimization problem, which jointly considers RIS assignment, entanglement distribution, and entanglement purification under the conflicting and interdependent constraints, including limited QBS capacity, UE fidelity thresholds and hard demands, and RIS service limitations. To the best of our knowledge, this is the first attempt in the literature to jointly consider all the above factors in RIS-assisted FSO-based QNs. The problem aims to maximize the total weighted demand size across all UE-RIS associations. To tackle this, we propose a 2-approximation algorithm, which leverages a tailored linear programming (LP) rounding technique. Finally, simulation results show that the proposed algorithm outperforms the existing baselines.

II. System Model and Problem Formulation

A. System Model

We consider a terrestrial FSO-based quantum network consisting of a QBS, a set of RISs $K = \{k_0, k_1, ..., k_{|K|-1}\}$, and a set of UEs $I = \{i_1, i_2, ..., i_{|I|}\}$. For notation consistency, k_0 denotes a direct path from the QBS to a UE without using any RIS. The QBS can generate entangled pairs at a rate of $r_{max} \in \mathbb{R}^+$ and distribute them to each UE $i \in I$ through a selected path either directly k_0 or via the reflection of some RIS $k \neq k_0$. Each RIS $k \in K$ can serve at most $c(k) \in \mathbb{Z}^+$ UEs at the same time from its coverage $I_k \subseteq I$. The length of path (i, k) is denoted by $l(i, k)$, which includes both the QBS-to-RIS and RIS-to-UE segments if $k \neq k_0$, or the QBS-to-UE length if $k = k_0$. The success probability of distributing an entangled pair along path (i, k) follows an exponential decay model based on path length [15]:

$$P_e(i, k) = e^{-\alpha \cdot l(i,k)}, \tag{1}$$

where α is a channel-dependent attenuation coefficient. The fidelity of the entangled pair over path (i, k) is assumed to follow the binary state and is modeled as [16]:

$$F_e(i, k) = \frac{1}{2} + \frac{1}{2} e^{-\beta \cdot l(i,k)}, \tag{2}$$

where β is a coefficient that captures decoherence effects, such as dephasing and detector imperfections [10], [17].

To improve the fidelity of low-quality entangled links, we apply entanglement purification [1], [13]. This process merges two entangled pairs with fidelity F_1 and F_2, where one is treated as the target and the other as a sacrifice pair. The success probability of purification is given by [16]:

$$P_p(F_1, F_2) = F_1 \times F_2 + (1 - F_1) \times (1 - F_2), \tag{3}$$

Upon success, the resulting fidelity of the target pair becomes:

$$F_p(F_1, F_2) = \frac{F_1 \times F_2}{F_1 \times F_2 + (1 - F_1) \times (1 - F_2)}. \tag{4}$$

In contrast, if purification fails, both input pairs are consumed.

To further improve the entanglement quality, we adopt a recursive purification technique, *pumping* [1], [16], where a target entangled pair is purified iteratively with multiple sacrifice pairs. Let $F(i, k, n)$ and $P(i, k, n)$ be the fidelity and success probability of executing $n \in \mathbb{Z}_0^+$ rounds of pumping purification using $n + 1$ entangled pairs between the QBS and UE i via RIS k, respectively. They are recursively defined as:

$$F(i, k, n) = \begin{cases} F_p(F(i, k, n-1), F_e(i, k)) & \text{if } n \geq 1 \\ F_e(i, k) & \text{if } n = 0 \end{cases} \tag{5}$$

$$P(i, k, n) = \begin{cases} P_p(F(i, k, n-1), F_e(i, k)) \\ \qquad \times P(i, k, n-1) & \text{if } n \geq 1 \\ 1 & \text{if } n = 0 \end{cases} \tag{6}$$

Eqs. (5) and (6) describe the recursive computation of fidelity and success probability under pumping, where each round builds on the results of previous purification rounds.

Given a specific path (i, k) for UE $i \in I$, the minimum number of required input pairs to generate one purified entangled pair that meets the fidelity threshold $\mathcal{F}(i) \in \mathbb{R}^+$ is:

$$n(i, k) = \min\{n \in \mathbb{Z}_0^+ \mid F(i, k, n) \geq \mathcal{F}(i)\}. \tag{7}$$

Let $d(i)$ denote the expected number of successful entangled pairs per unit of time demanded by UE i. To meet this hard

[1] Due to the page limit, related works are summarized in Appendix A [14].

demand using path (i,k), the QBS must distribute entangled pairs to that path at a rate of:

$$s(i,k) = \frac{(n(i,k)+1)\cdot d(i)}{P_e(i,k)\cdot P(i,k,n(i,k))}. \tag{8}$$

Note that the UE's demand is satisfied only if the allocated rate equals or exceeds $s(i,k)$. Finally, each UE $i \in I$ is associated with a weight $w(i) \in \mathbb{R}^+$.

B. Problem Formulation – REAP

Following the above system model, we formulate the Joint **R**IS Assignment, **E**nt**a**nglement Distribution, and **P**urification Problem (REAP) as an integer linear programming (ILP). The goal is to jointly determine the UE-RIS assignment and entangled pair distribution such that the total weighted demand size between UEs and RISs is maximized. To this end, we define decision variable $x_{ik} \in \{0,1\}$ indicating whether UE $i \in I$ is assigned to the path directly from the QBS or via RIS $k \in K \setminus \{k_0\}$. The REAP can be formulated as follows.

$$\max \quad \sum_{k\in K}\sum_{i\in I_k} w(i)\cdot d(i)\cdot x_{ik} \tag{9a}$$

$$\text{s.t.} \quad \sum_{k\in K}\sum_{i\in I_k} s(i,k)\cdot x_{ik} \le r_{max} \tag{9b}$$

$$\sum_{k\in K: i\in I_k} x_{ik} \le 1, \qquad \forall i \in I \tag{9c}$$

$$\sum_{i\in I_k} x_{ik} \le c(k), \qquad \forall k \in K \tag{9d}$$

$$x_{ik} \in \{0,1\}, \qquad \forall k \in K, \forall i \in I_k \tag{9e}$$

The objective (9a) maximizes the total weighted demand size for all satisfied UEs, ensuring that each satisfied UE can fully obtain the required entanglement rate in expectation. The constraint (9b) bounds the total distribution rate within the QBS capacity. The constraints (9c) and (9d) ensure that each UE is connected to at most one RIS, and each RIS serves at most $c(k)$ UEs. Note that the REAP is NP-hard, and the proof is provided in Appendix B [14] due to the page limit.

Theorem 1. The REAP is NP-hard.

III. Algorithm Design – RELIC

To efficiently solve the REAP, we design a 2-approximation algorithm, named Joint **R**IS Assignment and **E**ntang**l**ement **D**istribution With Purifi**c**ation Algorithm (RELIC), based on LP relaxation and rounding. For ease of reading, before introducing the RELIC, we transform the original instance into a theoretically equivalent one where each RIS can only serve one UE. We create such an instance by replicating each RIS $k \in K$ into $\min\{c(k), |I_k|\}$ identical RISs, each of which can serve only one UE in I_k. It is trivial to show that the instance transformation can be done in polynomial time. Thus, the RELIC only needs to consider those instances where each RIS can serve only one UE in the remainder of this section.

To achieve LP rounding, we relax the binary variable x_{ik} in the ILP (9a)–(9e) to $x_{ik} \ge 0$ between each RIS $k \in K$ and each UE $i \in I_k$. Then, we add one more constraint $(r_{max} - s(i,k))\cdot x_{ik} \ge 0, \forall k \in K, \forall i \in I_k$, ensuring that the QBS has sufficient capacity to fully serve UE i via RIS k if $x_{ik} > 0$. The relaxed LP can be solved in polynomial time by the existing LP solver (e.g., Gurobi). After acquiring the optimum LP solution, we then round it to an integral solution. For ease of presentation, we define $\tilde{x}_{ik}$ and $v(i)$ to denote the optimum LP solution and $w(i)\cdot d(i)$, respectively, in the following.

Intuitively, iteratively selecting the UE-RIS edge with the highest $\tilde{x}_{ik}$ (i.e., rounding it to one) tends to yield a higher total weighted demand size. However, this naive approach may make some UE i have no edge even if $\sum_{k\in K: i\in I_k} \tilde{x}_{ik} = 1$ due to constraints (9b) and (9d). This will result in a huge gap to the optimum LP solution since such UEs are more preferable than others for the optimum LP solution. To identify such UEs, we define the *UE fulfillment level (UFL)* $U(i) = \sum_{k\in K: i\in I_k} \tilde{x}_{ik}$ to indicate the optimum LP solution's preference for each UE i; it could be *fully served* (i.e., $U(i) = 1$), *partially served* (i.e., $U(i) \in (0,1)$), and *unserved* (i.e., $U(i) = 0$). Subsequently, we consider only the fully and partially served UEs. Thus, we construct an auxiliary edge-weighted graph $\tilde{G} = (\tilde{I} \cup \tilde{K}, \tilde{E})$, where $\tilde{I}$ represents all fully and partially served UEs, $\tilde{K}$ includes all RISs k with $\sum_{i\in \tilde{I}\cap I_k} \tilde{x}_{ik} > 0$, and $\tilde{E}$ denotes all the edges between UE $i \in \tilde{I}$ and RIS $k \in \tilde{K}$ with $\tilde{x}_{ik} > 0$. Also, the weight of each edge in $\tilde{E}$ indicates the required distribution rate $s(i,k)$. In other words, $\tilde{G}$ discards all the unserved UEs and zero-valued edges.

To design an efficient rounding method, we begin with a preprocessing step. Specifically, the UE-RIS edges with $\tilde{x}_{ik} = 1$ are included in the rounded solution. Then, we only need to consider the UE-RIS edges with $\tilde{x}_{ik} \in (0,1)$. $\tilde{G}$ may consist of disjoint cycles or paths. We first perform a transfer operation as follows. At each iteration, we identify a cycle or a *maximal extended path*[2] in $\tilde{G}$, and then incrementally shift a small fraction of the value $\tilde{x}_{ik}$ from even edges to odd edges or from odd edges to even edges, along the cycle or the maximal extended path. An edge will be selected into the rounded solution if its $\tilde{x}_{ik}$ reaches 1, and excluded from $\tilde{E}$ if $\tilde{x}_{ik}$ becomes 0. This shifting operation is repeatedly applied until no further edge's $\tilde{x}_{ik}$ can be transferred. The iteration terminates when every cycle or path is enumerated.

Let Δv and Δs denote the changes in weighted demand and distribution rate, respectively, after the transfer operation. During this operation, four possible cases arise: 1) $\Delta v = 0$, $\Delta s = 0$, 2) $\Delta v = 0$, $\Delta s < 0$, 3) $\Delta v > 0$, $\Delta s > 0$, and 4) $\Delta v < 0$, $\Delta s < 0$. In the first and second cases, we directly return the integral solution (i.e., all the UE nodes in $\tilde{G}$ are fully served, each served by only one RIS). If there are some UE nodes in $\tilde{G}$ unrounded and partially served, then we discuss the following cases. However, the third and fourth cases may yield an infeasible solution violating the QBS capacity or a solution far from the optimal solution. To address this, we select a specific UE from $\tilde{I}$ as the *pivot* and then derive two candidate solutions using the minimum weight matching algorithm and a customized greedy strategy, respectively; the first candidate

[2] A maximal extended path is a path that starts from any node and extends one hop at a time in both directions, until no further extension is possible.

does not include the pivot, while the second one does. Note that we choose the transfer operation leading to a lower total distribution rate (i.e., the fourth case) to avoid the third case.

Specifically, the partially served UE $i \in \tilde{I}$ that has an edge $(i,k) \in \tilde{E}$ with the highest $s(i,k)$ is elected as the pivot, i.e.,

$$p = \underset{i \in \tilde{I}:\, U(i) \in (0,1)}{\arg\max} \left(\max_{k \in \tilde{K}:\, (i,k) \in \tilde{E}} s(i,k) \right). \tag{10}$$

The first candidate solution includes all the UE-RIS edges selected in the minimum weight matching for the subgraph of $\tilde{G}$, extracted by removing the pivot p and its incident edges from $\tilde{G}$. Afterward, the second candidate using a customized greedy strategy first selects the edge between the pivot p and its RIS with the highest $s(p,k)$ and then iteratively selects the UE-RIS edges included in the first candidate with the highest ratio of $\frac{v(i)}{s(i,k)}$, referred to as the *cost-efficiency index (CEI)*, until the QBS capacity runs out. Finally, we choose the candidate with a higher total weighted demand size as the final solution.

The proposed RELIC comprises two main phases: 1) Fractional Solution Transfer (FST) and 2) Final Solution Generation (FSG). The FST performs the transfer operation to round some $\tilde{x}_{ik}$ values to 1. Then, the FSG generates two candidate solutions for the case involving partially served UEs. Finally, the candidate with a larger total weighted demand size is selected. The following subsections detail the two phases.

A. Fractional Solution Transfer (FST)

After obtaining the optimum LP solution, the FST constructs the auxiliary graph $\tilde{G} = (\tilde{I} \cup \tilde{K}, \tilde{E})$, where the nodes and edges are the fully and partially served UEs and their edges with $\tilde{x}_{ik} > 0$, respectively. First, all UE-RIS edges with $\tilde{x}_{ik} = 1$ are included in the rounded solution and excluded from the transfer. Then, the FST iteratively performs a transfer operation. In each iteration, the FST employs depth-first search (DFS) from any UE in $\tilde{G}$ to identify a cycle or a maximal extended path in $\tilde{G}$. For each identified one, a small fraction can be transferred from even edges to odd edges, or vice versa, along the cycle or maximal extended path in $\tilde{G}$. Both operations can turn one edge's $\tilde{x}_{ik}$ to 0 or 1. The FST chooses the one that leads to a lower total distribution rate (i.e., $\Delta s \leq 0$), and the shift repeats until no further edge value can be transferred. The iteration ends when every cycle or path is enumerated.

In addition, the remaining edges with $\tilde{x}_{ik} \in (0,1)$ may involve equivalence conditions across different components, under which the weighted demand and distribution rate remain unchanged after certain transfer operations of $\tilde{x}_{ik}$ among the edges. To eliminate these conditions, we then perform cross-component transfers to incrementally complete the assignment as fully as possible if these edges are equivalent. After the transfer, if $\Delta v = 0$ and each UE node in $\tilde{G}$ are fully served by exactly one RIS, then the FST directly return the integral solution, which corresponds to the optimal UE-RIS assignment.

Fig. 3 illustrates an example of the transfer operation. Each edge between a fully served UE and a RIS is labeled with its fractional value $\tilde{x}_{ik}$. Note that each RIS can only be connected to one UE. In Fig. 3(a), UE i_1 is fully served by RIS k_1 with $\tilde{x}_{i_1 k_1} = 1$ and is thus excluded from further processing. The

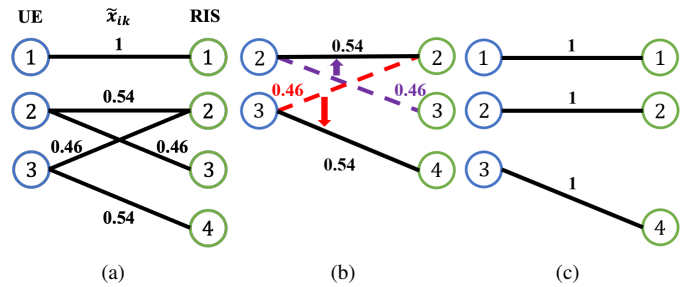

Fig. 3. An example of transfer operation.

DFS is then performed to identify a maximal extended path as shown in Fig. 3(b). The transfer operation that yields a lower total distribution rate is chosen. In this case, the values $\tilde{x}_{i_2 k_3}$ and $\tilde{x}_{i_3 k_2}$ of the odd edges (i_2, k_3) and (i_3, k_2), both equal to 0.46, are rounded down to 0, while the two even edges' values $\tilde{x}_{i_2 k_2}$ and $\tilde{x}_{i_3 k_4}$, both equal to 0.54, are rounded up to 1. After this operation, all UEs are satisfied by a single edge. The final optimal UE-RIS assignment is shown in Fig. 3(c).

B. Final Solution Generation (FSG)

For the case where some UEs in $\tilde{G}$ are partially served (i.e., the case of $\Delta v < 0$ and $\Delta s < 0$), the FSG generates two candidate solutions considering the pivot p. A partially served UE that has an edge $(i,k) \in \tilde{E}$ with the highest $s(i,k)$ is first elected as p. The edges associated with the partially served UEs, rather than p, together with those of the fully served UEs in $\tilde{G}$, are then used, based on their distribution rates $s(i,k)$, to construct a one-to-one assignment between UEs and RISs that minimizes the total distribution rate. This assignment is computed using the Hungarian algorithm [18] and serves as the first candidate solution. Fig. 4(a)–4(c) illustrates an example of the first candidate solution, with each edge's $\tilde{x}_{ik}$ value listed in Table I. The weighted demand and distribution rate of the optimum LP solution are 18.4 and 30, respectively. After the transfer operation, shown as orange lines in Fig. 4(a), the weighted demand and distribution rate become 17 and 18, respectively. Among the UEs, only UE i_4 is partially served now. Since UE i_4 has the highest $s(i,k) = 20$, it is elected as p, as shown in Fig. 4(a). The remaining edges (without p) in Fig. 4(b) are then processed using the Hungarian algorithm [18] to obtain the UE-RIS assignment with the minimum total rate. The first candidate solution is shown in Fig. 4(c).

The FSG generates the second candidate solution including the pivot p. Specifically, the selected edges from the first candidate solution are sorted in non-increasing order of their CEIs. The edge between pivot p and its RIS k with the highest $s(p,k)$, along with the sorted edges, are sequentially included until the QBS capacity runs out. Finally, we select the candidate solution with a higher total weighted demand size as the final solution. In Fig. 4(d), UE i_4 is selected as p and its incident edge (p,k) is added first to the second candidate solution. The selected edges from the first candidate solution, as shown in Fig. 4(c), are then sorted in descending order of their CEIs. Specifically, edges (i_1, k_1), (i_3, k_2), and (i_2, k_3) have CEIs of $\frac{5}{3}$, $\frac{6}{5}$, and $\frac{6}{10}$, respectively, satisfying the order $\frac{5}{3} > \frac{6}{5} > \frac{6}{10}$. After selecting edges (i_1, k_1) and (i_3, k_2), the total distribution

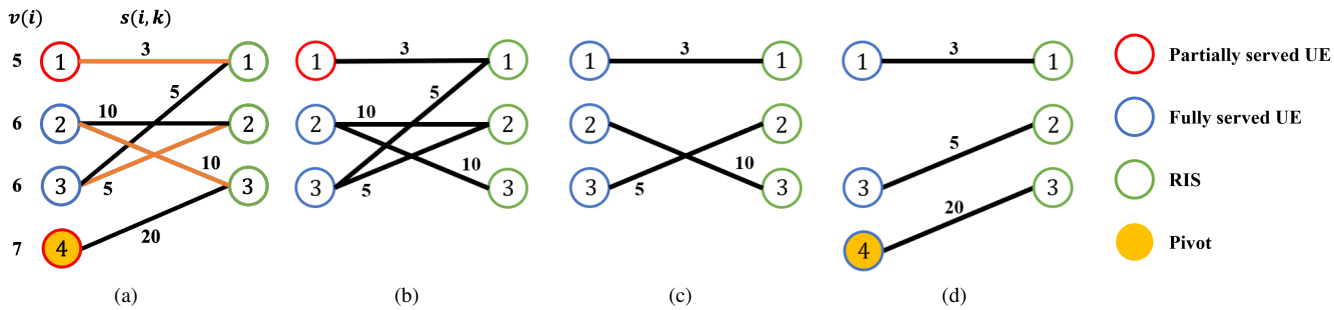

Fig. 4. An example of some UEs partially served, where $r_{max} = 30$.

TABLE I
VALUE OF $\tilde{x}_{ik}$

	$\tilde{x}_{i_1k_1}$	$\tilde{x}_{i_2k_2}$	$\tilde{x}_{i_2k_3}$	$\tilde{x}_{i_3k_1}$	$\tilde{x}_{i_3k_2}$	$\tilde{x}_{i_4k_3}$
Value	0.3	0.7	0.3	0.7	0.3	0.7

rate reaches 28, which would exceed the capacity if edges (i_2, k_3) were also selected. The second candidate solution is shown in Fig. 4(d), where the total weighted demand size is 18. Finally, the second candidate is adopted as the final solution since it has a higher total weighted demand size than the first one. Note that the RELIC is an approximation algorithm. Due to the page limit, the proof is detailed in Appendix C [14].

Theorem 2. The RELIC is a 2-approximation algorithm.

IV. PERFORMANCE EVALUATION

A. Simulation Settings

1) Network Generation: The network is generated as follows. A single QBS is positioned at coordinates $(0, 0, 90)$ within a 800×800 m^2 region, where UEs are deployed over the horizontal plane at a fixed height of 10 m, following a non-uniform random distribution, while RISs are uniformly randomly distributed at a fixed height of 90 m. The number of UEs and RISs are set to 50 and 15, respectively. In the 3D plane, each RIS is assigned a random orientation angle $\phi_k \in [0, 2\pi)$, indicating the direction of its surface normal. A UE is considered to be covered by a RIS only if it lies within the RIS's effective reflection sector, defined by an angular range $[\phi_k - \frac{\theta}{2}, \phi_k + \frac{\theta}{2}]$, where $\theta = 180°$.

2) Parameter Settings: The QBS entanglement generation rate is set to 10^7 pairs per unit of time. The expected number of successful entangled links demanded by each UE per unit of time is randomly selected from the range of $[10^5, 10^6]$. The probability of successful entanglement and the initial entangled fidelity are computed by Eqs. (1) and (2), where α and β are set to 0.0002 and 0.0044 [15], [17]. The required fidelity threshold for each UE is randomly drawn from a uniform distribution over $[0.7, 0.9]$ [19]. Following [20], we model the weight $w(i)$ of each UE as its willingness to pay (WTP) for the demand resource. Since entangled pairs are limited, UEs may compete for access. According to auction theory, the bidding prices of customers typically follow a normal distribution. Therefore, the WTP values are randomly generated from the right half of a normal distribution with a median of 1 and a standard deviation of 1.5, within a normalized range $[1, 3]$. The final weight of each UE i thus reflects its willingness to pay, ensuring that UEs with a higher WTP are assigned proportionally higher weights.

3) Baselines: We compare the performance of the proposed RELIC with four baselines. **1) Highest Ratio First (HRF)**: associates UEs and RISs in non-increasing order of CEIs until the QBS capacity runs out. **2) Highest Value First (HVF)**: selects UEs by descending order of $v(i)$, and each UE is assigned to the RISs with the lowest $s(i, k)$ until the QBS capacity runs out. **3) Simulated Annealing (SA)**: associates UEs and RISs by the metaheuristic [10]. **4) OPT**: uses Gurobi to derive the optimal solution of ILP (9a)−(9e). In addition, each simulation result is averaged over 100 trials.

B. Numerical Results

Fig. 5 shows the effects of various parameters on the different performance metrics. The RELIC jointly determines RIS assignment and entanglement distribution with purification to achieve the highest total weighted demand size, outperforming others. The results are explained in detail as follows.

1) Effect of Numbers of UEs/RISs: Fig. 5(a)–5(d) illustrate the impact of varying numbers of UEs/RISs on the total weighted demand size, total distribution rate, and number of satisfied UEs. In Fig. 5(a), the total weighted demand size increases slightly with the number of UEs, as a larger pool offers a higher likelihood of selecting valuable UEs. However, Fig. 5(b) exhibits no clear increasing or decreasing trend in the total distribution rate. This is because most methods, except for the SA, tend to fully utilize the available capacity. Subsequently, Fig. 5(c) demonstrates that the total weighted demand size increases with the number of RISs, as more RISs enable the system to serve a greater number of UEs (as shown in Fig. 5(d)). As a result, the HRF preferring high-CEI UE-RIS assignment misses high-$v(i)$ UEs, the HVF prioritizing high-$v(i)$ UEs neglects CEI, and the SA fails to consider purification, leading to worse performance. In contrast, our proposed RELIC can achieve a higher total weighted demand size close to the OPT through effective UE-RIS assignment, while maintaining efficient rate distribution, thus successfully mitigating the second and third challenges.

2) Effect of QBS capacity: Fig. 5(e) and 5(f) present how the total weighted demand size and the total distribution rate evolve with increasing QBS capacity. A larger capacity allows the QBS to serve more UEs, providing more flexibility in RIS assignment and resource allocation. Compared to the other methods, our RELIC can efficiently distribute the additional

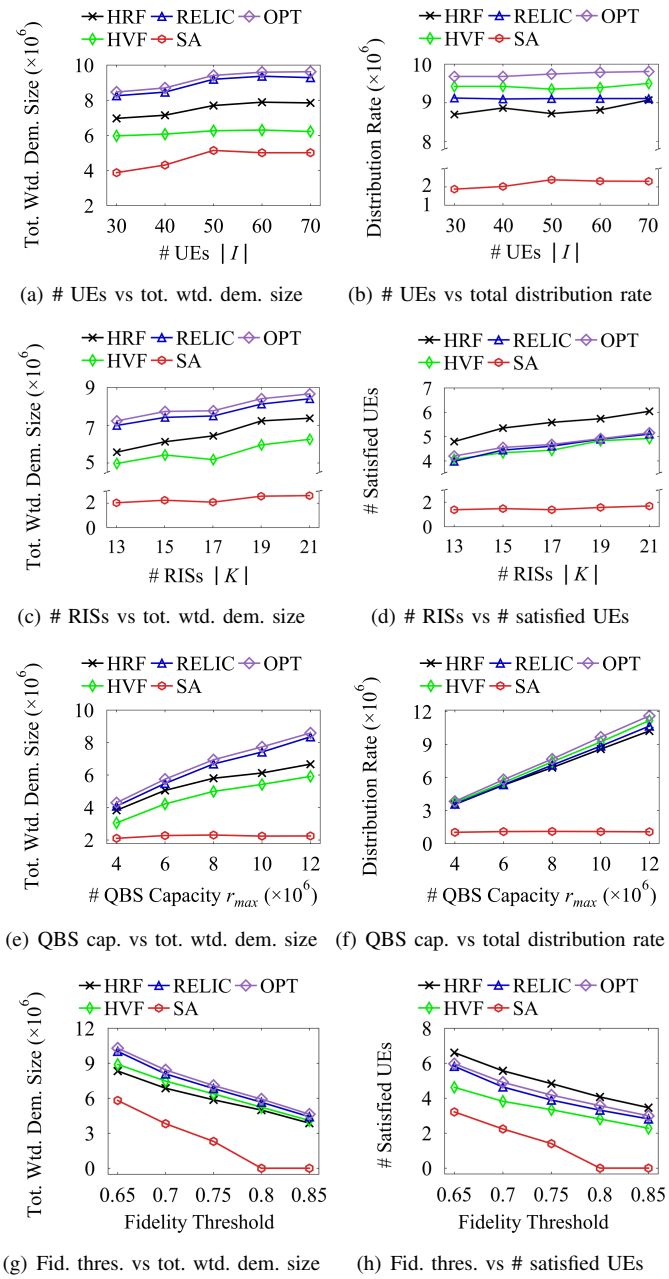

(a) # UEs vs tot. wtd. dem. size (b) # UEs vs total distribution rate

(c) # RISs vs tot. wtd. dem. size (d) # RISs vs # satisfied UEs

(e) QBS cap. vs tot. wtd. dem. size (f) QBS cap. vs total distribution rate

(g) Fid. thres. vs tot. wtd. dem. size (h) Fid. thres. vs # satisfied UEs

Fig. 5. Effects of different parameters on different metrics.

available resources by selecting more valuable UE-RIS assignments to satisfy UE demands, leading to a higher total weighted demand size and addressing the second challenge.

3) Effect of Fidelity Threshold: Fig. 5(g) and 5(h) display the values of the total weighted demand size and the number of satisfied UEs under the effect of different ranges of fidelity threshold. For each experiment, the individual fidelity threshold of each UE is randomly sampled from a uniform interval $[f_{\min}, f_{\min} + 0.05]$, where $f_{\min} \in \{0.65, 0.7, 0.75, 0.8, 0.85\}$ represents the lower bound of the tested range. As the fidelity threshold increases, the required number of purification rounds also escalates. In contrast to other algorithms, without implementing purification, the SA fails to meet most fidelity requirements, resulting in a drastic drop in both the demand size and the satisfied UEs. Compared to all the other algorithms, our proposed RELIC achieves a higher total weighted demand size close to the OPT, efficiently solving the first challenge.

V. Conclusion

In this paper, we address an optimization problem termed REAP, which jointly determines RIS assignment, entanglement distribution, and purification to maximize the total weighted demand size across all UEs. To solve this problem, we propose a 2-approximation algorithm named RELIC with two phases: FST and FSG. In the FST, the transfer operation is performed to round some $\tilde{x}_{ik}$ values to 1. The FSG then generates the two candidate solution considering the pivot for the case of some UEs partially served. Finally, the candidate solution with the highest total weighted demand size is selected as the final solution, which guides the QBS in establishing entangled links with UEs via selected RISs. Simulation results show that the proposed RELIC outperforms the other baselines by up to 67%.

References

[1] R. Van Meter, *Quantum Networking*. John Wiley & Sons, Ltd, 2014.

[2] S. Shi and C. Qian, "Concurrent entanglement routing for quantum networks: Model and designs," in *ACM SIGCOMM*, 2020.

[3] M. Chehimi *et al.*, "Entanglement rate optimization in heterogeneous quantum communication networks," in *ISWCS*, 2021.

[4] Y.-A. Chen *et al.*, "An integrated space-to-ground quantum communication network over 4,600 kilometres," *Nature*, vol. 589, no. 7841, pp. 214–219, 2021.

[5] L. Mazzarella *et al.*, "Quarc: Quantum research cubesat—a constellation for quantum communication," *Cryptography*, vol. 4, no. 1, p. 7, 2020.

[6] N. Hosseinidehaj *et al.*, "Satellite-based continuous-variable quantum communications: State-of-the-art and a predictive outlook," *IEEE Commun. Surv. Tutorials*, vol. 21, no. 1, pp. 881–919, 2019.

[7] H. Zhao and M.-S. Alouini, "On the transmission probabilities in quantum key distribution systems over FSO links," *IEEE Trans. Commun.*, vol. 69, no. 1, pp. 429–442, 2021.

[8] A. Dhiman *et al.*, "Classical-quantum signaling via stokes parameters," in *IEEE GLOBECOM*, 2024.

[9] N. K. Kundu *et al.*, "Intelligent reflecting surface-assisted free space optical quantum communications," *IEEE Trans. Wirel. Commun.*, vol. 23, no. 5, pp. 5079–5093, 2024.

[10] M. Chehimi *et al.*, "Reconfigurable intelligent surface (RIS)-assisted entanglement distribution in FSO quantum networks," *IEEE Trans. Wirel. Commun.*, vol. 24, no. 4, pp. 3132–3148, 2025.

[11] M. Jung *et al.*, "Performance analysis of large intelligent surfaces (LISs): Asymptotic data rate and channel hardening effects," *IEEE Trans. Wirel. Commun.*, vol. 19, no. 3, pp. 2052–2065, 2020.

[12] A. Chauhan *et al.*, "RIS partition-assisted non-orthogonal multiple access (NOMA) and quadrature-NOMA with imperfect SIC," *IEEE Trans. Wirel. Commun.*, vol. 22, no. 7, pp. 4371–4386, 2023.

[13] J.-W. Pan *et al.*, "Entanglement purification for quantum communication," *Nature*, vol. 410, pp. 1067–1070, 2001.

[14] C.-A. Yang *et al.*, "Joint RIS assignment and entanglement distribution with purification in FSO-based quantum networks (appendix)," Apr 2025. [Online]. Available: https://reurl.cc/ZNNrKM

[15] G. Zhao *et al.*, "Segmented entanglement establishment with all-optical switching in quantum networks," *IEEE/ACM Trans. Netw.*, vol. 32, no. 1, pp. 268–282, 2024.

[16] N. K. Panigrahy *et al.*, "On the capacity region of a quantum switch with entanglement purification," in *IEEE INFOCOM*, 2023.

[17] T. van Leent *et al.*, "Long-distance distribution of atom-photon entanglement at telecom wavelength," *Phys. Rev. Lett.*, vol. 124, p. 010510, 2020.

[18] H. W. Kuhn, "The Hungarian method for the assignment problem," *Nav. Res. Logist. Q.*, vol. 2, no. 1-2, pp. 83–97, 1955.

[19] S. Massar *et al.*, "Optimal extraction of information from finite quantum ensembles," *Phys. Rev. Lett.*, vol. 74, pp. 1259–1263, 1995.

[20] Y. Lee *et al.*, "Quantum network utility: A framework for benchmarking quantum networks," *Proc. Natl. Acad. Sci.*, vol. 121, no. 17, p. e2314103121, 2024.

Appendix A
Related Work

FSO-based QNs are increasingly emerging as a promising research topic. Günthner *et al.* [1] investigated the feasibility of long-distance quantum signal transmission via FSO links from a satellite in geostationary Earth orbit to an optical ground station, considering the effects of Earth's gravitational potential and atmospheric turbulence. Zhao *et al.* [2] developed analytical models for transmission probabilities across three distinct scenarios in quantum key distribution (QKD) systems over FSO channels. Dhiman *et al.* [3] proposed a protocol that enables the coexistence of secure quantum communication and high-throughput classical communication, under minimal alterations in both infrastructure and energy input. However, these studies do not address LoS obstructions or scenarios where LoS is unavailable in QNs.

When a direct path is unavailable in an FSO-based QN, one possible approach is to introduce an intermediate point to establish a virtual LoS link between the two nodes. Liu *et al.* [4] deployed unmanned aerial vehicles (UAVs) as relay nodes to facilitate quantum entanglement distribution, while mitigating diffraction and link losses in free-space communications. In [5], [6], satellites were utilized as relay nodes to support FSO-based QNs. However, UAVs are constrained by limited energy capacity, which poses challenges for long-distance or duration operations. Additionally, their stability and control can be adversely affected by weather conditions. On the other hand, using satellites as relay nodes increases deployment costs and causes higher latency due to the extended transmission distances. Regardless of the active relay type, the quantum signals must be stored using additional quantum memory.

An efficient and cost-effective solution to the LoS challenge in FSO-based QNs is through the use of RIS. Unlike active relays, RISs (or satellites) can forward entangled pairs without the need for quantum memory, making them a practical and scalable option for extending quantum connectivity. Hosseinidehaj *et al.* [7] surveyed the extension of space-based quantum communication, highlighting the use of satellites as optical reflectors to support FSO-based QNs. Kundu *et al.* [8] applied RIS to single-user non-line-of-sight (NLoS) FSO QKD systems, considering different protocols. Their results show that the use of RIS is not only feasible but also enhances the key generation rate. Nevertheless, [8] addresses only the applicability of RIS in QKD systems. Chehimi *et al.* [9] further leveraged a simulated annealing metaheuristic to jointly optimize RIS placement and entanglement rate allocation, while ensuring fidelity requirements. However, [9] considers only one RIS and directly excludes entangled links with fidelity below a certain threshold, thus limiting the RIS connection options for UEs and lowering long-distance UE satisfaction.

Appendix B
Proof of Theorem 1

We prove the theorem by reducing the knapsack problem [10] to the REAP. Given a set of objects $O = \{a_1, ..., a_n\}$, with specified sizes $s(a) \in \mathbb{Z}^+$ and profits $p(a) \in \mathbb{Z}^+$, and a knapsack capacity $B \in \mathbb{Z}^+$, the knapsack problem asks for a subset of objects whose total size is bounded by B and total profit is maximized. To accomplish the reduction from the knapsack problem to the REAP, we have to show how to construct an instance of the REAP (i.e., K, I, $w(i)$, $d(i)$, $s(i,k)$, $c(k)$, r_{max}) for the knapsack problem. The construction steps are detailed as follows. For each object $a \in O$, we create a corresponding UE i and RIS k, and add them to I and K, respectively. The weighted demand $w(i) \cdot d(i)$ and the rate $s(i,k)$ are then set to the profit $p(a)$ and the size $s(a)$, respectively. The UE i is assigned to I_k, and thus, all other distribution rates $s(i,k')$ for $k' \neq k$ are set to ∞. In addition, $c(k)$ is set to 1. For a knapsack capacity B, we create a corresponding QBS capacity r_{max}. The above reduction can be done in polynomial time. In this way, the knapsack problem can be solved if the solution of the REAP can be found. However, the knapsack problem is NP-hard and can only be solved when P = NP. Therefore, the theorem holds.

Appendix C
Proof of Theorem 2

Let $\tilde{x}$, $\hat{x}$, and OPT denote the fractional solution obtained from the relaxed LP, the integral solution of the RELIC, and the optimal solution of the REAP, respectively. Based on the values $\tilde{x}$ and $\hat{x}$, we construct the auxiliary edge-weighted graphs $\tilde{G}$ and $\hat{G}$, respectively. After the transfer operation, in Lemma 1, we demonstrate that the integral solution can be categorized into four cases: 1) $\Delta v = 0$, $\Delta s = 0$, 2) $\Delta v = 0$, $\Delta s < 0$, 3) $\Delta v > 0$, $\Delta s > 0$, and 4) $\Delta v < 0$, $\Delta s < 0$. In the first and second cases, each UE in $\tilde{G}$ is fully served by exactly one RIS. However, in the third and fourth cases, there are some UEs in $\tilde{G}$ unrounded and partially served. In the following, we analyze the theoretical gap between the RELIC and the optimum.

In the first and second cases, we show that the integral solution coincides with the optimal solution. If all UEs in $\tilde{G}$ are fully served, then the corresponding integral solution $\hat{G}$ is optimal after iteratively transferring a small fraction of value $\tilde{x}_{ik}$ from even edges to odd edges, or vice versa, without increasing the total distribution rate, while preserving the total weighted demand size (Lemma 2). In the third and fourth cases, we show that the fractional solution $\tilde{G}$ contains at most two partially served UEs (Lemma 3). Specifically, $\tilde{G}$ consists of disjoint cycles and paths, each referred to as a component. Among these components, we show that at most one can contain partially served UEs; otherwise, it is possible to increase the total weighted demand size by transferring values $\tilde{x}_{ik}$ from a lower-CEI component to a higher-CEI one.

Within this component, we further prove that there are at most two partially served UEs. If three or more such UEs exist, then according to the remaining QBS capacity, a strictly greater total weighted demand size can be achieved by appropriately shifting values $\tilde{x}_{ik}$ from edges with lower CEI or lower value to those with higher CEI or higher value, respectively. Then, in Lemma 4, we show that the total distribution rate of the first candidate solution, excluding the pivot, remains within the QBS capacity. Finally, Lemmas 3 and 4 together yield the approximation ratio of 2 between the optimal solution and the RELIC's integral solution. The proofs are detailed as follows.

$$\tilde{x}_{ik} := \begin{cases} \tilde{x}_{ik} + \epsilon_1, & \text{if } (i,k) \in odd \text{ and } \sum\limits_{(i',k') \in odd} s(i',k') \leq \sum\limits_{(i',k') \in even} s(i',k') \\ \tilde{x}_{ik} - \epsilon_2, & \text{if } (i,k) \in odd \text{ and } \sum\limits_{(i',k') \in odd} s(i',k') > \sum\limits_{(i',k') \in even} s(i',k') \\ \tilde{x}_{ik} - \epsilon_1, & \text{if } (i,k) \in even \text{ and } \sum\limits_{(i',k') \in odd} s(i',k') \leq \sum\limits_{(i',k') \in even} s(i',k') \\ \tilde{x}_{ik} + \epsilon_2, & \text{if } (i,k) \in even \text{ and } \sum\limits_{(i',k') \in odd} s(i',k') > \sum\limits_{(i',k') \in even} s(i',k') \end{cases}, \text{where } \begin{array}{l} \epsilon_1 = \min\{\min\limits_{(i',k') \in even} \tilde{x}_{i'k'}, \min\limits_{(i',k') \in odd} 1 - \tilde{x}_{i'k'}\} \\ \epsilon_2 = \min\{\min\limits_{(i',k') \in odd} \tilde{x}_{i'k'}, \min\limits_{(i',k') \in even} 1 - \tilde{x}_{i'k'}\} \end{array} \tag{11}$$

Lemma 1. The integral solution after the transfer operation includes four cases: 1) $\Delta v = 0$, $\Delta s = 0$, 2) $\Delta v = 0$, $\Delta s < 0$, 3) $\Delta v > 0$, $\Delta s > 0$, and 4) $\Delta v < 0$, $\Delta s < 0$.

Proof. There are nine possible cases in total. For $\Delta v > 0$, we have $\Delta s = 0$, $\Delta s < 0$, and $\Delta s > 0$. The first two cases imply that the relaxed LP solution is not optimal, whereas the third case is valid since $\Delta s > 0$ may result in $\Delta v > 0$. For $\Delta v < 0$, we again have $\Delta s = 0$, $\Delta s < 0$, and $\Delta s > 0$. The first and third cases are invalid, as their counterparts under $\Delta v > 0$—namely, $\Delta v > 0$ with $\Delta s = 0$ and $\Delta v > 0$ with $\Delta s < 0$—do not exist. For $\Delta v = 0$, we also have $\Delta s = 0$, $\Delta s < 0$, and $\Delta s > 0$. The last case is excluded because we select the transfer operation that yields a lower total distribution rate. Therefore, the lemma holds. □

In the first and second cases, each UE in $\tilde{G}$ is fully served by exactly one RIS. We then demonstrate the existence and optimality of the two cases by Lemma 2 as follows.

Lemma 2. If all UEs in $\tilde{G}$ are fully served, then the corresponding integral solution $\hat{G}$ is optimal for the REAP.

Proof. After eliminating cycles and equivalence conditions, every maximal extended path must start and end at a RIS node. We prove it by contradiction. Assume that a maximal extended path p starts or ends at a UE node, denoted by i. Let k denote the RIS node on p connected to UE node i. There are two possible cases: 1) the incident edge (i,k) on p has a fractional allocation of $\tilde{x}_{ik} \in (0,1)$, and 2) it has an integral allocation of $\tilde{x}_{ik} = 1$. For case 1, UE i must have another edge (i,k') with $\tilde{x}_{ik'} > 0$ since UE i is fully served. Such an edge (i,k') can extend path p further, leading to a contradiction since p is a maximal extended path. For case 2, if the incident edge (i,k) has $\tilde{x}_{ik} = 1$, then p includes only edge (i,k). It does not need adjustment or rounding and would not form a maximal extended path. As a result, every maximal extended path must start and end at a RIS node.

After identifying a maximal extended path with length at least 2, we can transfer a fractional value $\tilde{x}_{ik}$ from even edges to odd edges, or vice versa. At each iteration, the values are updated by transferring a small amount ϵ_1 or ϵ_2, as shown in Eq. (11). By determining the appropriate ϵ_1 or ϵ_2 as in Eq. (11), this guarantees the feasibility of $\tilde{x}_{ik}$. Each of these transfer operations can convert the fractional value of at least one edge to either 0 or 1. Among the two resulting configurations, we select the one that yields an equal or lower total distribution rate. Since the fully served UE i satisfies $U(i) = \tilde{x}_{ik_1} + \tilde{x}_{ik_2} = 1$, where k_1 and k_2 are two different connected RISs, it follows that the adjusted allocations still satisfy $U(i) = 1$. Specifically, $\tilde{x}_{ik_1} + \epsilon_1 + \tilde{x}_{ik_2} - \epsilon_1 = 1$ when $s(i,k_1) \leq s(i,k_2)$, and $\tilde{x}_{ik_1} - \epsilon_2 + \tilde{x}_{ik_2} + \epsilon_2 = 1$ when $s(i,k_1) > s(i,k_2)$. In both cases, the total distribution rate does not increase: $(\tilde{x}_{ik_1} + \epsilon_1) \cdot s(i,k_1) + (\tilde{x}_{ik_2} - \epsilon_1) \cdot s(i,k_2) \leq \tilde{x}_{ik_1} \cdot s(i,k_1) + \tilde{x}_{ik_2} \cdot s(i,k_2)$ if $s(i,k_1) \leq s(i,k_2)$, and similarly for the reverse case. These ensure that the resulting integral solution $\hat{G}$ achieves the same total weighted demand size without increasing the total distribution rate. Therefore, the lemma holds. □

Subsequently, we analyze the gap between the optimum OPT and the integral solution $\hat{G}$ in the fourth case, including two candidate solutions. To establish the approximation ratio, we first show that $\tilde{G}$ contains at most two partially served UEs, as stated in Lemma 3. Then, in Lemma 4, we demonstrate that the total distribution rate of the first candidate solution, excluding the pivot, remains within the QBS capacity. These two lemmas together yield the desired approximation ratio.

Lemma 3. The fractional solution $\tilde{G}$ contains at most two UEs that are partially served.

Proof. After eliminating cycles and equivalence conditions, the fractional solution $\tilde{G}$ consists of disjoint paths, each referred to as a component. Among these components, it suffices to show that at most one can contain partially served UEs. Assume that $\tilde{G}$ contains two components, each with a partially served UE connected to a RIS, and that this assignment achieves the highest total weighted demand size under the limited QBS capacity. However, based on their respective CEIs, a new assignment with a higher objective value can be constructed by allocating more distribution rate to the edge with the higher CEI, and assigning the remaining rate to the other edge. This results in only one partially served UE. Since the edge with the higher CEI yields greater value per unit rate, the objective value increases, leading to a contradiction. Therefore, at most one component in $\tilde{G}$ can contain partially served UEs.

Within this component, we further show that there can be at most two partially served UEs. Assume that there are three such UEs connected to the same RIS. If these UEs were connected to different RISs, the fractional allocations could be shifted toward the edge with the higher CEI, resulting in a strictly higher total weighted demand size. Therefore, the only case that requires consideration is when all partially served UEs are connected to a single RIS, and their corresponding edges have increasing values and rates arranged in non-increasing order of their CEIs. Assume further that this assignment achieves the highest total weighted demand size under the limited QBS capacity and RIS connection. However, a new assignment with a higher objective value can be constructed by leveraging the remaining QBS capacity. Based on their respective CEIs, the following analysis considers five distinct situations:

1) If the remaining capacity is only sufficient to fully satisfy the edge with the highest CEI, then reallocating the fractional allocations from the other two edges to it can yield a greater objective value, resulting in no partially served UE.

2) If the remaining capacity is sufficient to fully satisfy the edge with the highest CEI while still leaving capacity, then reallocating the fractional allocation from the edge with the *lowest CEI* to the other two edges can yield a greater objective value, resulting in two partially served UEs.

3) If the remaining capacity is sufficient to fully satisfy the edge with the second-highest CEI, then reallocating the fractional allocations from the other two edges to it can yield a greater objective value and leave no partially served UE.

4) If the remaining capacity is sufficient to fully satisfy the edge with the second-highest CEI while still leaving capacity, then reallocating the fractional allocation from the edge with the *lowest value* to the other two edges can yield a greater objective value, resulting in two partially served UEs.

5) If the remaining capacity is sufficient to fully satisfy the edge with the third-highest CEI, then reallocating the fractional allocations from the other two edges to it can yield a greater objective value, resulting in no partially served UE.

From the above cases, there are at most two partially served UEs, leading to a contradiction. Therefore, the lemma holds. □

Lemma 4. The total distribution of the first candidate solution, excluding the pivot, does not exceed the QBS capacity.

Proof. If there is only one partially served UE in $\tilde{G}$, it is selected as the pivot, and the first candidate solution consists of all other fully served UEs. According to Lemma 2, their total distribution rate does not exceed the QBS capacity after rounding to an integral solution. If there are two partially served UEs in $\tilde{G}$, then by Lemma 3, they must be connected to the same RIS, and satisfy $U(i_1) + U(i_2) = 1$, where i_1 and i_2 denote the two partially served UEs. Following our algorithm, the UE with the higher-rate edge is selected as the pivot. The first candidate solution then includes the other UE with its edge fully rounded, i.e., $\tilde{x}_{ik} = 1$. Since the lower distribution rate satisfies $\min\{s(i_1,k), s(i_2,k)\} \leq U(i_1) \cdot s(i_1,k) + U(i_2) \cdot s(i_2,k)$, the total distribution rate of the first candidate solution remains within the QBS capacity. Therefore, the lemma holds. □

Let $\hat{G}_1$ and $\hat{G}_2$ represent the first and second candidate (integral) solutions, respectively. Let $\tilde{e}$ be the edge between the pivot UE p and its connected RIS k, where $\tilde{x}_{pk} \in (0,1)$. The corresponding edge in the rounded solution is denoted by $\hat{e}$, where $\tilde{x}_{pk} = 1$. Let $v(G)$ denote the total weighted demand size of a solution G, and $v(\{e\})$ denote the weighted demand size associated with a single edge e. Then, we have

$$\begin{aligned} v(\tilde{G}) &= v(\tilde{G} \setminus \{\tilde{e}\}) + v(\{\tilde{e}\}) \\ &\leq v(\hat{G}_1) + v(\{\hat{e}\}) \\ &\leq v(\hat{G}_1) + v(\hat{G}_2). \end{aligned} \tag{12}$$

The first inequality holds for two reasons: 1) $\hat{G}_1$ is a feasible one-to-one assignment between UEs and RISs by Lemma 4, and thus its objective value is at least as high as that of $\tilde{G} \setminus \{\tilde{e}\}$. 2) The objective value of $\tilde{e}$ is strictly less than that of $\hat{e}$. The second inequality holds because $\hat{G}_2$ includes other edges from the first candidate solution. By (12), we obtain

$$\frac{1}{2} \cdot v(\tilde{G}) \leq \max\{v(\hat{G}_1), v(\hat{G}_2)\}. \tag{13}$$

Recall that OPT denote the optimal solution of the REAP. It is correct that the objective value of the optimal fractional solution is no less than that of the optimal (integral) solution, i.e.,

$$OPT \leq v(\tilde{G}). \tag{14}$$

Finally, we have the total weighted demand size at most:

$$OPT \leq 2 \cdot \max\{v(\hat{G}_1), v(\hat{G}_2)\}. \tag{15}$$

Therefore, the theorem holds. In the following, we analyze the time complexity of the proposed RELIC.

Time Complexity. The second phase dominates the overall time complexity. Specifically, in the FST phase, the DFS of the transfer operation takes $O(|\tilde{I}| + |\tilde{K}| + |\tilde{E}|)$ time. In the FSG phase, the Hungarian algorithm [11] to find an integral matching requires $O((\max\{|\tilde{I}|, |\tilde{K}|\})^3)$ time. The FSG phase then takes $O(|\tilde{E}| \log |\tilde{E}|)$ and $O(1)$ time, respectively, to sort the selected edges from first candidate solution and select the final solution. Therefore, the overall time complexity of the proposed RELIC is $O((\max\{|\tilde{I}|, |\tilde{K}|\})^3)$. ■

References

[1] K. Günthner *et al.*, "Quantum-limited measurements of optical signals from a geostationary satellite," *Optica*, vol. 4, no. 6, pp. 611–616, 2017.

[2] H. Zhao and M.-S. Alouini, "On the transmission probabilities in quantum key distribution systems over FSO links," *IEEE Trans. Commun.*, vol. 69, no. 1, pp. 429–442, 2021.

[3] A. Dhiman *et al.*, "Classical-quantum signaling via stokes parameters," in *IEEE GLOBECOM*, 2024.

[4] H.-Y. Liu *et al.*, "Optical-relayed entanglement distribution using drones as mobile nodes," *Phys. Rev. Lett.*, vol. 126, p. 020503, 2021.

[5] Y.-A. Chen *et al.*, "An integrated space-to-ground quantum communication network over 4,600 kilometres," *Nature*, vol. 589, no. 7841, pp. 214–219, 2021.

[6] L. Mazzarella *et al.*, "Quarc: Quantum research cubesat—a constellation for quantum communication," *Cryptography*, vol. 4, no. 1, p. 7, 2020.

[7] N. Hosseinidehaj *et al.*, "Satellite-based continuous-variable quantum communications: State-of-the-art and a predictive outlook," *IEEE Commun. Surv. Tutorials*, vol. 21, no. 1, pp. 881–919, 2019.

[8] N. K. Kundu *et al.*, "Intelligent reflecting surface-assisted free space optical quantum communications," *IEEE Trans. Wirel. Commun.*, vol. 23, no. 5, pp. 5079–5093, 2024.

[9] M. Chehimi *et al.*, "Reconfigurable intelligent surface (RIS)-assisted entanglement distribution in FSO quantum networks," *IEEE Trans. Wirel. Commun.*, vol. 24, no. 4, pp. 3132–3148, 2025.

[10] V. V. Vazirani, *Approximation Algorithms*. Springer, 2003.

[11] H. W. Kuhn, "The Hungarian method for the assignment problem," *Nav. Res. Logist. Q.*, vol. 2, no. 1-2, pp. 83–97, 1955.